Supporting Information

Proton Reservoir in Polymer Photocatalysts for the Superior H_2O_2 Photosynthesis

Bo Sheng,[abc] Yangen Xie,[ab] Qi Zhao,[ab] Hua Sheng*[ab] and Jincai Zhao[ab]

[a] Key Laboratory of Photochemistry, Institute of Chemistry Chinese Academy of Sciences, Beijing National Laboratory for Molecular Sciences, Beijing 100190, P.R. China

[b] University of Chinese Academy of Sciences, Beijing 100049, P.R. China

[c] National & Local Joint Engineering Research Center for Deep Utilization Technology of Rock-salt Resource, Faculty of Chemical Engineering, Huaiyin Institute of Technology, Huai'an, Jiangsu 223003, P.R. China

Table of Contents

Text S1 **Chemicals**

Ethanol, sodium iodate, monobasic potassium phosphate, potassium phosphate, sulfuric acid, H_2O_2, ethyl acetate, benzyl alcohol, iron powder (Fe^0) and tetracycline were analytic grade and acquired by Sino pharm Chemical Reagent Co., Ltd., China. 5,5-dimethyl-1-pyrroline-Noxide (DMPO) was purchase from Dojindo Laboratories. 2,2,6,6-Tetramethyl-4-piperidone hydrochloride (TEMP) was obtained from Tokyo Chemical Industry. N,N-Dimethylacetamide (DMAC), N,N-diethyl-1,4-phenylene-diamine (DPD), peroxidase (POD), polyvinylidene difluoride (PVDF), benzoquinone (BQ), and 3,3',4,4'-Tetraaminobiphenyl (DAB) were provided by Aladdin. The sponge was purchased from the Internet.

Text S2 Synthesis of Quinone-Amine polymers (QAPs)

QAPs were synthesized via a facile precipitation polymerization method. Typically, 1 mmol of 3,3'-diaminobenzidine (DAB) was dissolved in ethanol (40 mL) with a round-bottomed flask, and then the mixture was heated to 70 °C. Subsequently, to obtained QAPs in different contents of hydroquinone units, varied amounts (1, 2, 4, 5 and 8 mmol for QAP_1, QAP_2, QAP_4, QAP_5 and QAP_8, respectively) of BQ (dissolved in 30 mL ethanol) was slowly added under stirring. After 8 h reaction, the obtained precipitants were separated and washed with ethyl acetate and ethanol. Finally, the brown solid samples was dried under vacuum at 60 °C overnight.

Text S3 **Materials characterizations**

The scanning electron microscopy (SEM) images were performed on Hitachi S-4800 microscope. A Hitachi UV–vis spectrophotometer (UV-3900) equipped with an integrating sphere was used to record the UV-vis absorption of materials. $BaSO_4$ was selected as the reflectance standard. Time-resolved photoluminescence (TRPL) spectra were performed on a Hamamatsu Quantaurus-TauC11367 spectrophotometer with an excitation wavelength at 365 nm at room-temperature. Powder X-ray diffraction (PXRD) patterns of the samples were collected on a analytical B.V. X-ray powder diffractometer with CuKα radiation (2θ range from 5° to 45°). ^{13}C MAS NMR spectra were collected on a Bruker Avance III 400 MHz spectrometer at room temperature. The N_2 adsorption-desorption experiments were conducted on a Quantachrome Autosorb IQ Instruments. Electron paramagnetic resonance (EPR) spectra were recorded on a Bruker Elexsys E500-T spectrometer at room temperature.

Text S4 **Electrochemical tests**

All electrochemical experiments were conducted on a CHI760E electrochemical workstation (CH Instrument Co.,), using a standard three-electrode system in 0.5 M Na_2SO_4 at room temperature. The Pt wire and Ag/AgCl electrode was used as the counter and reference electrodes, respectively. QAPs polymer (1.2 mg) were dispersed in 150 μL ethanol, and then 15 μL of Nafion solution (5 wt. %) was added into the dispersion followed by ultrasonic treatment for 30 min. 30 μL of the resultant ink was drop-coated onto a FTO glass, which was heated at 60 °C in vacuum overnight.

For RRDE measurements (Pine Research Instrument, USA), QAPs polymer (0.5 mg) were dispersed in 150 μL ethanol, and then 15 μL of Nafion solution (5 wt. %) was added to the dispersion followed by ultrasonic treatment for 10 min. 3 μL of the resultant ink was drop-coated onto a glassy carbon disk electrode (OD: 5.6 mm) and dried at room temperature. The linear sweep scan was conducted at 20 mV/s in O_2-saturated 0.1 M phosphate buffer solution (pH = 7.0). The working electrode was rotated at a speed of 400, 700, 1000, 1300 and 1600 rpm, respectively. The electron transfer number (n) for oxygen reduction was calculated by Koutechy-Levich equation:

$$\frac{1}{j} = \frac{1}{j_k} + \frac{1}{B\omega^{0.5}}$$

$$B = 0.62 \times n \times F \times D_{O_2}^{2/3} \times v^{-1/6} \times C_{O_2}$$

where j is the current density, ω means the rotation speed, n is the number of electrons transferred during the reaction; D_{O2} and C_{O2} are diffusion coefficient of O_2 and bulk concentration of O_2, respectively; F represents the Faraday constant and ν is the dynamic viscosity of the electrolyte.

Text S5 **H_2O_2 photosynthesis**

The H_2O_2 photosynthesis on QAPs was conducted as follows: 10 mg of QAPs were dispersed in 50 mL pure water and sonicated for 2 min. After stirring in dark for 10 min, the obtained suspension was irradiated by a 300 W Xenon lamp (λ > 420 nm) with continuous air or pure O_2 flow (0.1 L·min^{-1}), the temperature of photosynthesis system was controlled at 25 °C. 2 mL of suspension was filtrated with a 0.22 μm filtration membrane at desired intervals. The concentration of H_2O_2 was measured by N,N-diethyl-1,4-phenylene-diamine (DPD) and peroxidase (POD) method.[1] The details were as follows: 2 mL sample was added into the mixture of 3 mL water and 0.4 mL phosphate buffer, followed by the addition of 50 μL DPD. Finally, the obtained solution was shaken after the addition of 50 μL POD, then the concentration of H_2O_2 in the solution was determined by the absorbance at 551 nm in UV-vis spectrum.

The solar-to-chemical conversion (SCC) efficiency of photocatalytic H_2O_2 production by QAPs was performed under simulated solar light irradiation (AM1.5 global spectrum). The SCC efficiency was calculated by the following equation:[2]

$$\text{SCC efficiency} = \frac{\Delta G^0 \times n(H_2O_2)}{(total\ input\ energy) \times (reaction\ time)} \times 100\%$$

Where ΔG^0 is the free energy for H_2O_2 generation (117 kJ·mol^{-1}), n(H_2O_2) is the molar of the formed H_2O_2 (mol), the overall irradiance of the AM1.5 global spectrum is 1000 W·m^{-2}, and the irradiation area is about 0.4 × 10^{-4} m^2.

To calculate the apparent quantum yield (ΦAQY), the incident light was passed through a monochromator. The ΦAQY was calculated by the following equation:

$$\Phi AQY\ (\%) = \frac{number\ of\ H_2O_2 molecules \times 2}{number\ of\ incident\ photons} \times 100\%$$

Text S6 **Radicals detection**

In-suit experiments were conducted on a Bruker model electron spin resonance (ESR) E500-T spectrometer equipped with an external light resource. DMPO and TEMP were selected the spin trapper of $^{\bullet}OH$ and $O_2^{\bullet-}$, respectively. Generally, 1 mL solution of catalyst (0.2 g·L^{-1}) was added into a centrifugation tube followed by the addition of spin trapper (100 mM), after variously shaking, certain amounts of suspensions were loaded into a capillary tube and subsequently an NMR tube for the EPR measurement at room temperature. For the measurement of solid powders, 20 mg of QAPs was directly loaded into the NMR tube.

Text S7 Measurement of in-situ FTR analysis

In-situ Fourier transform infrared (FTIR) spectra were recorded on a Bruker Vertex 70 V spectrometer equipped with narrow-band HgCdTe detector cooled by liquid nitrogen. The diffusion IR mode (DRIFTs) was employed and connected to an evacuation line (~0 hPa). The QAP sample was pressed into a pellet (7 mm in diameter) with BaF_2 as diluent. The sample was placed into the DRIFTs chamber and evacuated overnight. During the IR measurement, dry O_2 was first introduced to monitor the interaction between QAPs and O_2, after then, water-saturated O_2 was used instead. After the dark interaction between QAPs and O_2/water reached an equilibrium, the illumination started.. The light resource was a 150 mW continuous diode laser (375 nm). The in-situ IR spectrum with a spectral resolution of 4 cm^{-1} and scanning velocity of 160 KHz was collected in both of the dark and illumination period.

Text S8 The application of QAP-based H_2O_2 photosynthesis

To test the activity of QAP in real aquatic environment, tape water and natural water (collected

sample from the lake in Haidian Park, Beijing) was employed instead of deionized water (18.2 MΩ·cm^{-1}), the natural water was sampled from a lake in Haidian Park in Beijing.

To build up a floatable photocatalytic platform for the pollutant degradation, QAP was loaded on the floatable sponge supporter. To be specific, 0.3 g PVDF was dissolved in 20 mL DMAC solution and stirred for 1 h at 50 °C, after then, 10 mL solution was transferred into centrifuge tube containing 100 mg QAP (mixture A), and 5 mL solution was transferred into centrifuge tube containing 100 mg Fe^0 (mixture B). After shaking 3 mins, the mixture A and B was drop-coated on the upper and lower surface of sponge (6 × 6 cm^2), respectively. During the degradation of tetracycline hydrochloride (TC, concentration: 20 mg·L^{-1}), the floated platform was upon the illumination of 300 W Xenon lamp ($\lambda >$ 420 nm), and the concentration of the residue TC was determined by UV-Vis.

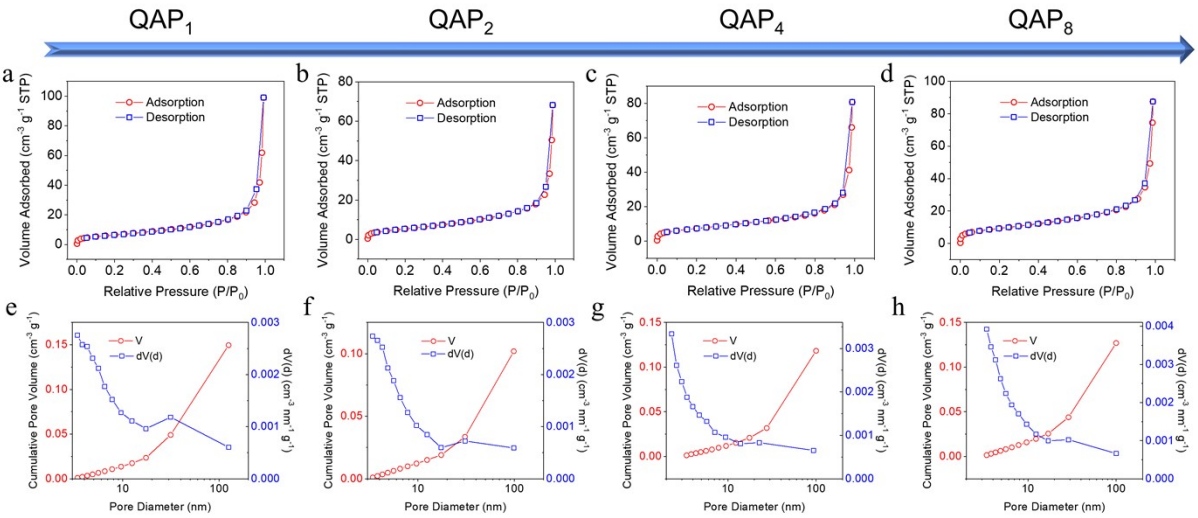

Fig. S1 Adsorption-desorption isotherms (a-d) and pore size distribution (e-h) of QAPs.

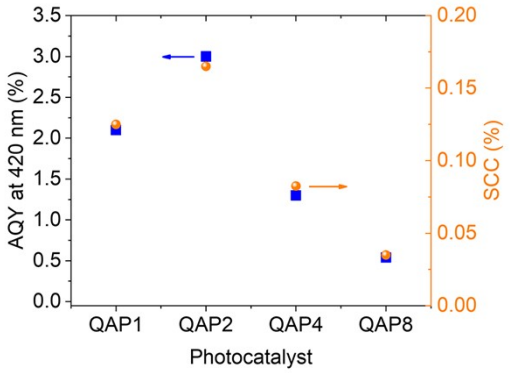

Fig. S2 The apparent quantum efficiency (AQY, left Y-axis) obtained through 420 nm illumination, and the solar-to-chemical conversion efficiency (SCC, right Y-axis) under AM 1.5 G irradiation for different QAP photocatalysts.

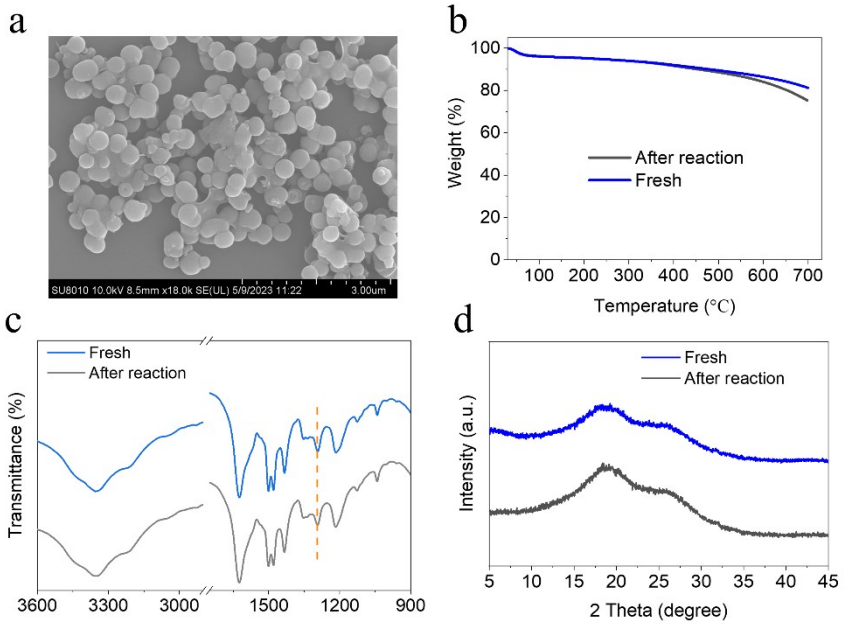

Fig. S3 The characterization of QAP_2 after reaction by (a) SEM, (b) TGA, (c) FT-IR, and (d) XRD.

The catalyst after reaction have been systematically characterized. No significant alternation was observed in SEM image. In FT-IR spectra, all the characteristic bands in fresh samples were both observed after photocatalytic reaction with remained intensity ratios, specifically the hydroquinone units (1292 cm^{-1}) were resistant to oxidation, preserving their integrity during the photoreactions No significant alternation was detected in XRD patterns. These results firmly proved the stability of QAP photocatalysts.

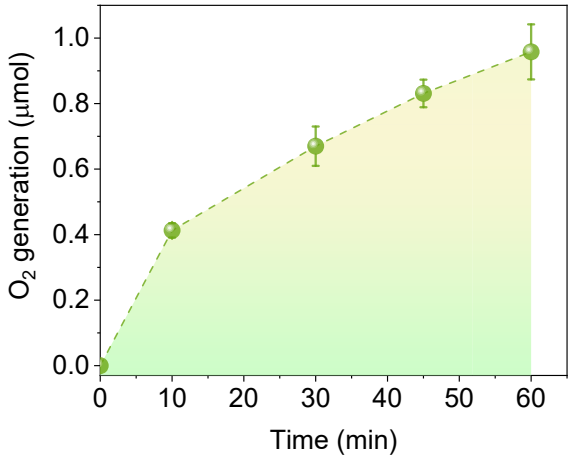

Fig. S4 Amounts of O_2 generated in WOR half photoreaction with $NaIO_3$ as an electron-scavenger. Conditions: water (50 mL), QAPs catalyst (10 mg), $NaIO_3$ (3 mM), Ar (1 bar), λ >420 nm (Xe lamp).

To clarify the origin of H_2O_2 produced by QAPs during photoreaction, we selected the QAP_2 as the target catalyst in half reactions with sacrificial reagents. With $NaIO_3$ as an electron-scavenger under Ar, the major WOR product was determined to be O_2 instead of H_2O_2 was detected, suggesting that the source of H_2O_2 generation was from WOR.

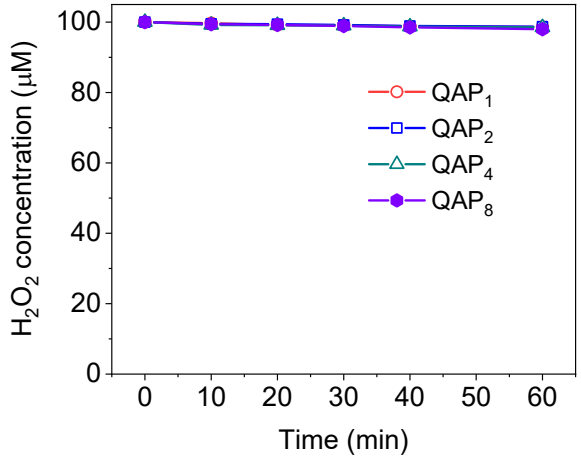

Fig. S5 The investigation for the decomposition of H_2O_2 by QAPs under illumination. Conditions: 10 mg catalysts, 50 mL water, 100 μM H_2O_2, 3 mM $NaIO_3$, Ar (1 bar), λ >420 nm (Xe lamp, 100 mW/cm^2).

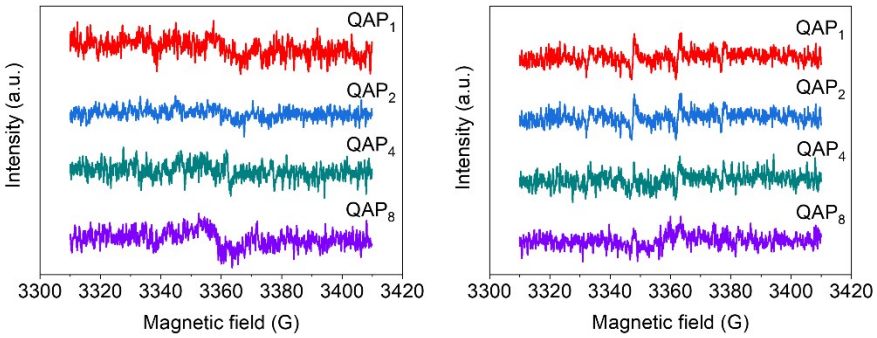

Fig. S6 The measurement of ROS species (a) $O_2^{\bullet-}$ and (b) $^{\bullet}OH$ by EPR during the photosynthesis of H_2O_2.

We used 5,5-dimethyl-1-pyrroline-N-oxide (DMPO) and 2,2,6,6-tetramethyl-4-piperidinoe (TEMP) as the spin-trap agents for the detection of $O_2^{\bullet-}$ and (b) $^{\bullet}OH$, in EPR, respectively. After 5 min illumination, the inconspicuous quadruple peak signals of DMPO-$^{\bullet}OH$ (1:2:2:1) for all QAPs excluded the formation of $^{\bullet}OH$ and its contribution to H_2O_2 production. The detected signal intensities of DMPO-$O_2^{\bullet-}$ were also minimal, disclosing the generation pathway of H_2O_2 from single electron-transfer as reported previously.

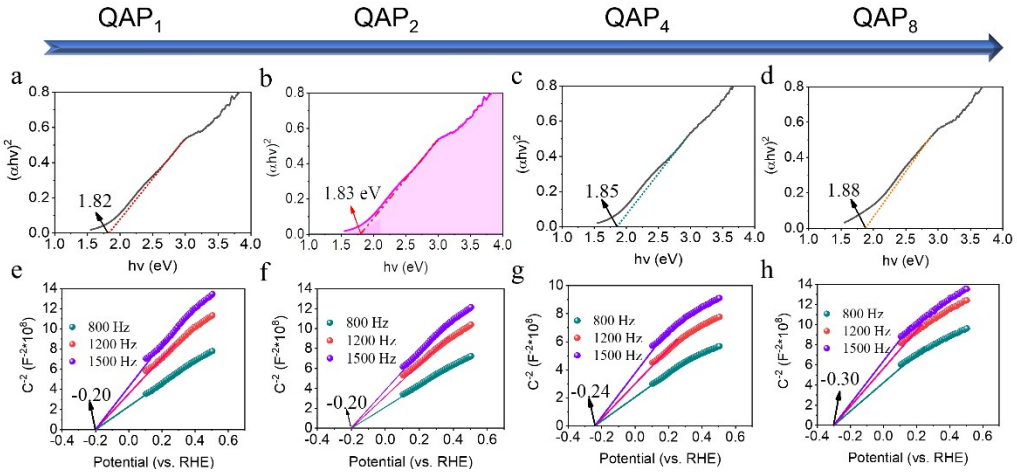

Fig. S7 Tauc plots (a-d), and Mott-Schottky curves (e-h) measured in 0.5 M Na_2SO_4 solution.

The bandgaps were calculated to be in the range from 1.82 to 1.88 eV, much lower than some artificial semiconductors (e.g., C_3N_4, COFs).[3,4] The positive tangent slope in Tauc plot indicates that the polymer is a n-type semiconductor. Together with the Mott−Schottky testing results, the conduction band (CB) and the valence band (VB) positions were calculated, respectively. Based on the band levels, it can be determined that QAPs favored ORR to produce H_2O_2 (H_2O_2/O_2, 0.67 V) and WOR to produce O_2 (H_2O/O_2, 1.23 V) but not for H_2O_2 (H_2O/H_2O_2, 1.73 V).

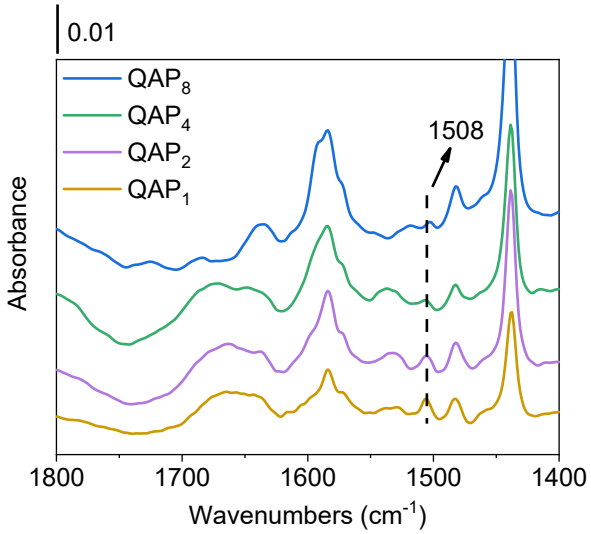

Fig. S8 In situ IR spectra for pyridine adsorbed on QAPs collected at room temperature.

Pyridine is generally used as probe to detect the Brönsted or Lewis acid sites on the catalysts. Based on the literature,[5,6] the peaks located at 1508 cm^{-1} can be assigned to the adsorption of pyridine on a Brönsted acid site. The intensities of these peaks decrease with the increase in BQ/DBA ratio from QAP_1 to QAP_8.

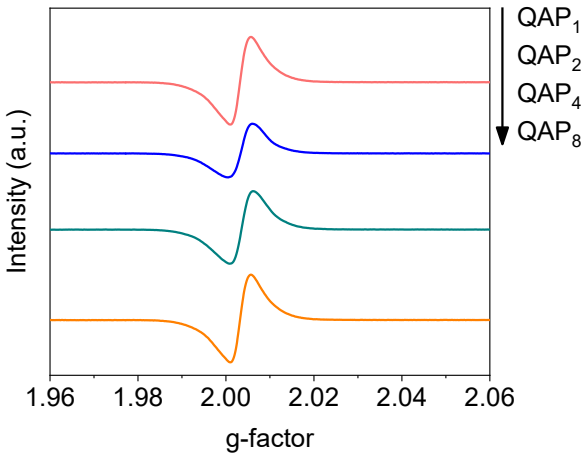

Fig. S9 The electron paramagnetic resonance (EPR) spectra of the QAPs in the dark conditions.

Table S1. Specific surface area of the samples and the pore size fitted through BJH model.

Photocatalysts	Surface Area (m^2/g)	Pore Volume (cc/g)	Pore Diameter Dv(d) (nm)
QAP_1	18.672	0.150	3.390
QAP_2	15.314	0.102	3.391
QAP_4	16.076	0.118	3.392
QAP_8	19.896	0.127	3.395

Table S2. Comparison of metal-free polymer-based photocatalysts for non-sacrificial H_2O_2 production.

Photocatalysts	H_2O_2 production (μmol/g/h)	Light source/ Volume of solution	Conditions	Reference
QAP_2	**380**	**λ >420 nm, 50 mL**	**Air, H_2O**	**This work**
PEI/C_3N_4	20.8	AM 1.5G, N.A.	O_2, H_2O	[7]
Dc-CTF	322	λ > 350 nm, 50 mL	O_2, H_2O	[8]
CNP-s	343.2	λ> 420nm, 30 mL	O_2, H_2O	[9]
Resin	82	λ> 420nm, 30 mL	O_2, H_2O	[10]
Py-Bpy-COF	241	N.A., 10 mL	O_2, H_2O	[11]
OCN-500	106	λ> 420nm, 15 mL	O_2, H_2O	[12]
NMT400	270	AM1.5G, 50 mL	O_2, H_2O	[13]
5Cv@g-C_3N_4	125	λ> 420nm, 10 mL	O_2, H_2O	[14]
rGO@MRF	86	λ> 420nm, 100 mL	O_2, H_2O	[15]
KCN-0.7	104	λ> 420nm, 50 mL	O_2, H_2O	[16]
CHF-DPDA	69	λ> 420nm, 20 mL	O_2, H_2O	[17]
FS-COFs	1501.6	λ> 420nm, 20 mL	O_2, H_2O	[18]
HEP-TAPT-COF	1750	λ> 420nm, 100 mL	O_2, H_2O	[19]
TPE-AC	293	λ> 400nm, 20 mL	Air, H_2O	[20]
RF-resin	160	λ> 400nm, 50 mL	Air, H_2O	[21]
OPCN	50	λ> 400nm, 50 mL	Air, H_2O	[22]

N.A.: not-available

References

1 H. Bader, V. Sturzenegger and J. Hoigné, *Water Res.*, 1988, **22**, 1109–1115.

2 H. Tan, P. Zhou, M. Liu, Q. Zhang, F. Liu, H. Guo, Y. Zhou, Y. Chen, L. Zeng, L. Gu, Z. Zheng, M. Tong and S. Guo, *Nat. Synth*, 2023, **2**, 557–563.

3 C. Ayed, J. Yin, K. Landfester and K. Zhang, *Angew. Chem. Int. Ed.*, 2023, **62**, e202216159.

4 R. Tang, D. Gong, Y. Zhou, Y. Deng, C. Feng, S. Xiong, Y. Huang, G. Peng, L. Li and Z. Zhou, *Appl. Catal., B*, 2022, **303**, 120929.

5 J. An, Y. Wang, J. Lu, J. Zhang, Z. Zhang, S. Xu, X. Liu, T. Zhang, M. Gocyla, M. Heggen, R. E. Dunin-Borkowski, P. Fornasiero and F. Wang, *J. Am. Chem. Soc.*, 2018, **140**, 4172–4181.

6 L. Ding, M. Li, Y. Zhao, H. Zhang, J. Shang, J. Zhong, H. Sheng, C. Chen and J. Zhao, *Appl. Catal., B*, 2020, **266**, 118634.

7 X. Zeng, Y. Liu, Y. Kang, Q. Li, Y. Xia, Y. Zhu, H. Hou, M. H. Uddin, T. R. Gengenbach, D. Xia, C. Sun, D. T. Mccarthy, A. Deletic, J. Yu and X. Zhang, *ACS Catal.*, 2020, **10**, 3697–3706.

8 C. Wu, Z. Teng, C. Yang, F. Chen, H. B. Yang, L. Wang, H. Xu, B. Liu, G. Zheng and Q. Han, *Adv. Mater.*, 2022, e2110266.

9 H. Yang, C. Li, T. Liu, T. Fellowes, S. Y. Chong, L. Catalano, M. Bahri, W. Zhang, Y. Xu, L. Liu, W. Zhao, A. M. Gardner, R. Clowes, N. D. Browning, X. Li, A. J. Cowan and A. I. Cooper, *Nat. Nanotechnol.*, 2023, **18**, 307–315.

10 Y. Shiraishi, T. Takii, T. Hagi, S. Mori, Y. Kofuji, Y. Kitagawa, S. Tanaka, S. Ichikawa and T. Hirai, *Nat. Mater.*, 2019, **18**, 985–993.

11 J. Sun, H. Sekhar Jena, C. Krishnaraj, K. Singh Rawat, S. Abednatanzi, J. Chakraborty, A. Laemont, W. Liu, H. Chen, Y.-Y. Liu, K. Leus, H. Vrielinck, V. van Speybroeck and P. van der Voort, *Angew. Chem. Int. Ed.*, 2023, **62**, e202216719.

12 Z. Wei, M. Liu, Z. Zhang, W. Yao, H. Tan and Y. Zhu, *Energy Environ. Sci.*, 2018, **11**, 2581–2589.

13 C. Yang, S. Wan, B. Zhu, J. Yu and S. Cao, *Angew. Chem. Int. Ed.*, 2022, **61**, e202208438.

14 L. Chen, C. Chen, Z. Yang, S. Li, C. Chu and B. Chen, *Adv. Funct. Mater.*, 2021, **31**, 2105731.

15 Q. Tian, X.-K. Zeng, C. Zhao, L.-Y. Jing, X.-W. Zhang and J. Liu, *Adv. Funct. Mater.*, 2023, **33**, 2213173.

16 J. Yue, H. Yang, C. Liu, Q. Zhang and Y. Ao, *Appl. Catal., B*, 2023, **331**, 122716.

17 H. Cheng, H. Lv, J. Cheng, L. Wang, X. Wu and H. Xu, *Adv. Mater.*, 2022, **34**, e2107480.

18 Y. Luo, B. Zhang, C. Liu, D. Xia, X. Ou, Y. Cai, Y. Zhou, J. Jiang and B. Han, *Angew. Chem. Int. Ed.*, 2023, e202305355.

19 D. Chen, W. Chen, Y. Wu, L. Wang, X. Wu, H. Xu and L. Chen, *Angew. Chem. Int. Ed.*, 2022, e202217479.

20 Y.-X. Ye, J. Pan, Y. Shen, M. Shen, H. Yan, J. He, X. Yang, F. Zhu, J. Xu, J. He and G. Ouyang, *Proc. Natl. Acad. Sci. U.S.A.*, 2021, **118**, e2115666118.

21 X. Zhang, J. Wang, B. Xiao, Y. Pu, Y. Yang, J. Geng, D. Wang, X. Chen, Y. Wei, K. Xiong and Y. Zhu, *Appl. Catal., B*, 2022, **315**, 121525.

22 F. Wang, J. Xu, Z. Wang, Y. Lou, C. Pan and Y. Zhu, *Appl. Catal., B*, 2022, **312**, 121438.